Seismic reliability evaluation of steel-timber hybrid shear wall systems

Zheng Li[*1], Minjuan He[1], Frank Lam[2], Ruirui Zhou[1] and Minghao Li[3]

[1]*Department of Structural Engineering, Tongji University, Shanghai, 200092, China*
[2]*Department of Wood Science, University of British Columbia, Vancouver, Canada*
[3]*Department of Civil & Natural Resources Engineering, University of Canterbury, Christchurch, New Zealand*

Abstract: This paper presents seismic performance and reliability evaluation on steel-timber hybrid shear wall systems composed of steel moment resisting frames and infill light frame wood shear walls. Based on experimental observations, damage assessment was conducted to determine the appropriate damage-related performance objectives for the hybrid shear wall systems. Incremental time-history dynamic analyses were conducted to establish a database of seismic responses for the hybrid systems with various structural configurations. The associated reliability indices and failure probabilities were calculated by two reliability methods (i.e., fragility analysis and response surface method). Both methods yielded similar estimations of failure probabilities. This study indicated the greatly improved seismic performance of the steel-timber hybrid shear wall systems with stronger infill wood shear walls. From a probabilistic perspective, the presented results give some insights on quantifying the seismic performance of the hybrid system under different seismic hazard levels. The reliability-based approaches also serve as efficient tools to assess the performance-based seismic design methodology and calibration of relative code provisions for the proposed steel-timber hybrid shear wall systems.

Keywords: steel-timber hybrid structures; seismic reliability; shear walls; fragility analysis; response surface method

1. Introduction

In order to provide an alternative for multi-story structural systems in seismic prone zones, a unique steel-timber hybrid structure has been proposed by He *et al.* (2014) and Li *et al.* (2016). The steel-timber hybrid structure is composed of steel moment-resisting frames and steel-timber hybrid diaphragms. Light wood frame shear walls are integrated as infill walls into the steel moment-resisting frames, forming a hybrid shear wall system to resist lateral loads. It should be noted that the infill wood shear walls provide a considerable contribution to the lateral resistance of the structure, thus the functionality of the wood shear walls in the hybrid structure is quite different from that of conventional non-structural infill walls. The steel-timber hybrid diaphragm is composed of C-shaped steel joists and dimension lumber decking with casted cement mortar on top to improve serviceability performance. The self-weight of the hybrid structure is largely reduced due to the application of wood elements. In the steel-timber hybrid buildings, most of the structural members are prefabricated, which can ensure the construction quality. Experimental studies also revealed that the infill wood shear walls were very effective in resisting lateral loads for the hybrid structural systems (He *et al.* 2014).

The seismic performance for other multi-story timber/timber-hybrid building systems has attracted much research attention in the past decade (Sakamoto *et al.* 2004,

Yamaguchi *et al.* 2004, Buchanan *et al.* 2008, Smith *et al.* 2009, Van de Lindt *et al.* 2011, Dickof *et al.* 2014, Tesfamariam *et al.* 2014, Zhang *et al.* 2016, Pozza and Trutalli 2017, Li *et al.* 2017a, b). There are also interests to quantify the seismic performance of building systems using probabilistic tools with reasonable performance-related criteria. Seismic reliability analyses of steel frame structures have been largely carried out by researchers (e.g., Kazantzi *et al.* 2008, 2011, Noh *et al.* 2012, Roeder *et al.* 2012). For wood shear wall systems, the seismic reliability analyses were also conducted (Foliente 2000, Filiatrault and Folz 2002, Wang and Foliente 2006, Li *et al.* 2009). However, no research has been conducted to study the seismic reliability of the proposed steel-timber hybrid shear wall systems.

In this paper, a verified numerical model is used to create a seismic response database for the steel-timber hybrid wall systems with different structural configurations. The seismic reliability of steel-timber hybrid shear walls is then evaluated by two approaches namely fragility method and response surface method. This study intends to provide a technical basis for quantifying the seismic performance of the steel-timber hybrid systems as well as the development of performance-based seismic design method and relative code provisions.

2. Hybrid shear wall configuration and numerical model

Fig. 1 shows the structural configuration of the baseline steel-timber hybrid shear wall used in this study. Mild carbon steel Q235B with cross sections of H-150 mm× 100 mm×6 mm×9 mm and H-150 mm×150 mm×7 mm×10 mm,

---

*Corresponding author, Ph.D.
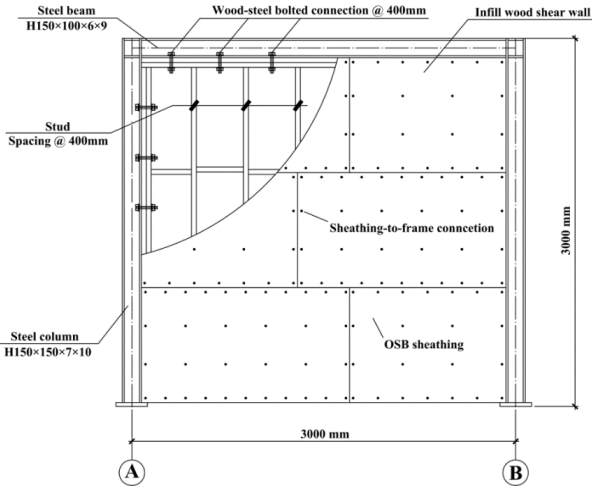E-mail: zhengli@tongji.edu.cn

Fig. 1 Steel-timber hybrid baseline wall

Fig. 2 "Pseudo nail" algorithm to model the infill wood shear walls

Fig. 3 FE model for timber-steel hybrid shear wall system

which are conforming to Chinese Standard GB 50017 (2003), were used for beams and columns in the steel frame. For the infill wood shear wall, No. 2 and better grade Spruce-Pine-Fir (SPF) 38 mm×140 mm dimension lumber with a spacing of 400 mm was used as framing members, and performance rated OSB panels were used as the sheathing material. Bolted connections were used to connect the top plate and side studs of the infill wall to the steel frame. The bolts transferred the shear force between the steel fame and the wood infill wall, and ensured that the infill wall and the steel frame could resist lateral load together. For infilled frame systems, the relative lateral infill-to-frame stiffness ratio has a crucial influence on its lateral performance (e.g., stiffness, loading resisting capacity, etc.). The lateral stiffness ratio Kr for an infilled frame system can be defined as the ratio of the elastic stiffness between the infill wall and the steel frame

$$K_r = k_{\text{infill}} / k_{\text{bf}} \qquad (1)$$

where $k_{\text{infill}} = 0.4 P_{\text{infill}} / \Delta_{\text{infill}}$ and $k_{\text{bf}} = 0.4 P_{\text{bf}} / \Delta_{\text{bf}}$, P_{infill} is the peak load resisted by the infill wood shear wall, kN; and Δ_{infill} is the lateral displacement of the infill wall at $0.4 P_{\text{infill}}$, mm; P_{bf} is the peak load resisted by the bare steel frame, kN; and Δ_{bf} is the lateral displacement of the bare steel frame at $0.4 P_{\text{bf}}$, mm. It should be noted that under severe ground motions, stiffness degradation may occur and affect the stiffness ratio; however, the calculation of K_r is based on

the elastic stiffness of the infill wall and the steel frame. In this study, the seismic performance of the hybrid shear walls with four K_r values (i.e., 0.5, 1.0, 2.5, and 5.0) was evaluated. The different K_r values were achieved by designing the hybrid shear wall systems with different nailing schedules & panel thickness, as listed in Table 1. These numbers cover a reasonable range in practical applications of the steel-timber hybrid systems. Other structural configurations, such as the wall geometry and the cross section of the steel members, remained the same for these hybrid shear walls.

A nonlinear finite element (FE) model was developed in ABAQUS software package by Li *et al.* (2014a) to simulate the seismic response of the steel-timber hybrid shear walls. As a general FE software package, ABAQUS does not have appropriate hysteretic elements to fully consider the strength and stiffness degradation and pinching effects of nail connections or wood shear walls. Thus, a so called "pseudo nail" algorithm was implemented into ABAQUS as a user defined subroutine to represent the hysteretic behavior of the infill wood shear wall. Considering the similar hysteretic characteristics between a wood shear wall and a nail connection, the "pseudo nail" model was proposed by Gu and Lam (2004) to represent the load-drift hysteresis of a wood shear wall using a nailed connection model, as shown in Fig. 2. Of course, the nailed connection model parameters need to be calibrated in order to match the magnitudes of actual shear wall forces and drifts. The details of the "pseudo-nail" model have been discussed by Li *et al.* (2009). The "pseudo nail" wall model has been shown to be computationally efficient and capable of modeling the behavior of wood shear walls under both

Table 1 Structural configurations of infill walls for different relative lateral infill-to-frame stiffness ratios

Kr	Nail type	Sheathing type	Sheathing pattern
0.5	CN50a	9.5mm OSB	One side
1.0	CN50	9.5mm OSB	Both sides
2.5	12d common nailb	14.7mm OSB	One side
5.0	12d common nail	14.7mm OSB	Both sides

Note: aCN50 nail is confirmed to the Japanese Industrial Standards (JIS), with 50 mm in length and 2.87 mm in diameter.
b12d common nail is confirmed to ASTM F1667-11a (Standard Specification for Driven Fasteners: Nails, Spikes, and Staples), with 82 mm in length and 3.8 mm in diameter.
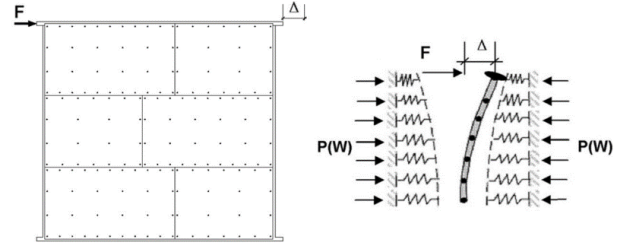
static and dynamic loads (Li and Lam 2009, Li *et al.* 2014b). The developed FE model for the steel-timber hybrid shear wall system in ABAQUS is shown in Fig. 3. Detailed information for the numerical model and its verification can be found in Li *et al.* (2014b).

3. Seismic input and performance objectives

In this study, high seismicity zone with design Intensity VIII was assumed according to Chinese Standard GB 50011 (2010), also known as CCSDB (Chinese Code for Seismic Design of Buildings). The soil condition was assumed to Type III with average shear wave velocity between 140 m/s and 250 m/s, representing a stiff soil condition. The design spectrum with respect to the seismic intensity and soil condition were determined using the detailed provisions in CCSDB. Since the strong historical ground motion data in China is still very limited, besides the selected Chinese records, several destructive records, most of which have similar soil conditions with the assumed site, were selected from the Pacific Earthquake Engineering Research Center's Next Generation Attenuation (NGA) database. The ground motion records used in this study are listed in Table 2.

CCSDB has also defined immediate occupancy (IO), life safety (LS) and collapse prevention (CP) limit states, and the 50-year exceedance probabilities for the earthquakes considered in the IO, LS and CP limit states are 63%, 10% and 2%, in accordance with the average return period of 50, 475, and 2475 years, respectively. The spectral accelerations corresponding to these hazard levels were 0.16, 0.45 and 0.90 g, respectively. These ground motion records were then scaled to seismic hazard levels via a response spectrum approach, i.e., the 5% damped spectral value over the plateau region (0.1-0.65 s) should match the design spectral value according to CCSDB.

In order to study the relationship between shear wall responses and seismic hazard levels, incremental time-
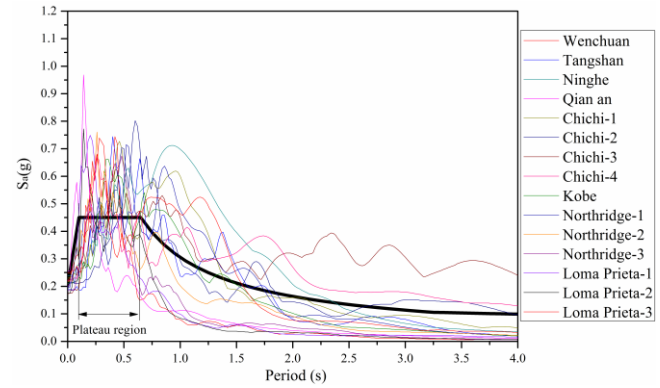

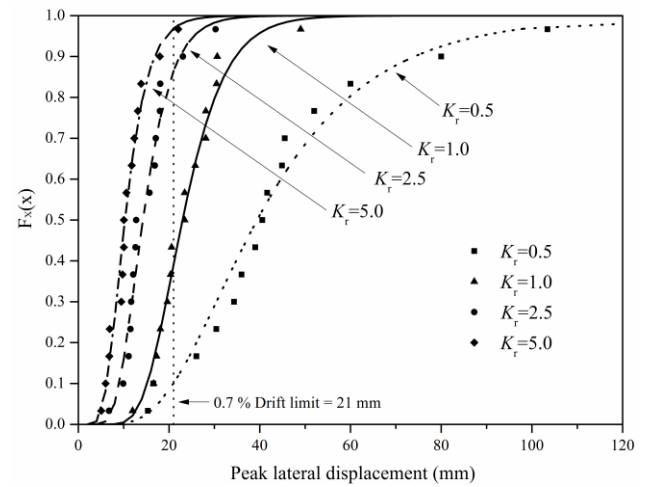Fig. 4 Ground motion records scaled over plateau region of the response spectrum (LS hazard level)

Fig. 5 Cumulative peak wall displacement distributions for hybrid shear walls with various Kr values under IO limit state

history analyses were performed at fifteen different spectral acceleration (Sa) levels (i.e., 0.10, 0.16, 0.30, 0.45, 0.60, 0.75, 0.90, 1.05, 1.20, 1.35, 1.50, 1.65, 1.80, 1.95 and 2.10 g), and the ground motion records were scaled to these spectral acceleration values, respectively. An example for the matching process for the LS hazard level (which is corresponding to the spectral acceleration of 0.45g) is shown in Fig. 4.

It is generally accepted in performance-based seismic engineering that deformation limit states tend to be straightforward measure which is related to both structural and non-structural damage. For steel moment resisting frames and wood shear walls, the inter-story drift provides a good estimate of the expected damage and a well-established compromise between local and global response measures. He *et al.* (2014) showed that both the wood shear walls and the steel moment frames provided significant contributions to resist lateral loads in the steel-timber hybrid shear wall systems. Although the CCSDB has defined the IO, LS and CP performance levels, there are still no code provisions on determining seismic performance objectives under these performance levels in China. Therefore, rational drift limits for the steel-timber hybrid shear wall systems were provided based on test results in He *et al.* (2014) and

Table 2 Ground motion records used in analysis

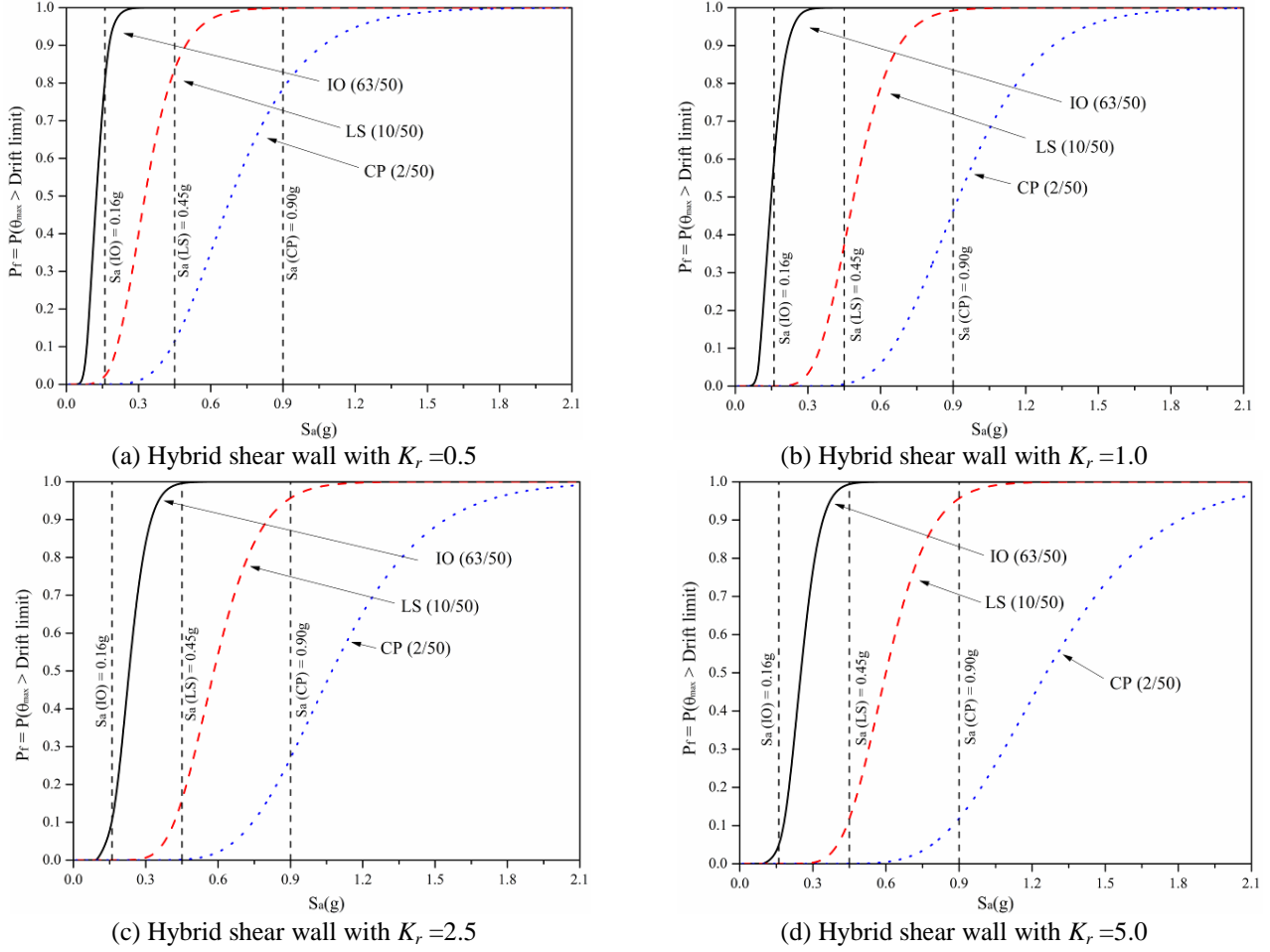| NO.	Event	Date	Station	Component	PGA (g)
1	Wenchuan	12/05/2008	Wolong	EW	0.976
2	Tangshan	28/071976	Beijing Hotel	EW	0.067
3	Ninghe	25/11/1976	Tianjin Hospital	NS	0.149
4	Qian'an	31/08/1976	M0303 Qianan lanhe bridge	NS	0.135
5	Chichi-1	21/09/1999	CHY006	NS	0.345
6	Chichi-2	21/09/1999	TCU070	EW	0.255
7	Chichi-3	21/09/1999	TCU106	NS	0.128
8	Chichi-4	21/09/1999	TAP052	NS	0.127
9	Kobe	17/01/1995	0 KJMA	KJM000	0.821
10	Northridge-1	17/01/1994	0013 Beverly Hills – 14145 Mulhol	MUL+009	0.416
11	Northridge-2	17/01/1994	24278 Castaic – Old Ridge Route	ORR090	0.568
12	Northridge-3	17/01/1994	90086 Buena Park – La Palma	BPK090	0.139
13	Loma Prieta-1	18/10/1989	47381 Gilroy Array #3	G03000	0.555
14	Loma Prieta-2	18/10/1989	57425 Gilroy Array #7	GMR000	0.226
15	Loma Prieta-3	18/10/1989	58224 Oakland – Title & Trust	TIB180	0.195

Fig. 6 Peak displacement fragility curves for different hazard levels: (a) Hybrid shear wall with K_r =0.5, (b) Hybrid shear wall with K_r =1.0, (c) Hybrid shear wall with K_r =2.5 and (d) Hybrid shear wall with K_r =5.0

the provisions in ASCE/SEI-41 (2013). A damage assessment procedure was firstly conducted as detailed described in (Li *et al.* 2014b), and the 0.7%, 2.5%, and 5.0% have been defined as the drift limit under the IO, LS, and CP performance levels, respectively.

4. Fragility analysis

Seismic fragility $F_{R(z)}$ describes the conditional probability of reaching or exceeding a specified deterministic or random performance level with an intensity measure z, and it is defined as

$$F_R(z) = P[G < 0 \mid IM = z] \qquad (2)$$

where G is the limit state function, and IM is the intensity measure consistent with the specific seismic hazard. In this study, IM equals to S_a, which is the spectral acceleration. Eq. (2) can be rewritten as Eq. (3) when taking into account that the inter-story drift as the performance criterion and the intensity measure.

$$F_R(z) = P[\theta_{max} \geq \theta_{PL} \mid S_a = z] \qquad (3)$$

where θ_{max} is the maximum inter-story drift from the

analysis, θ_{PL} is the drift limit according to different performance levels. It is quite convenient to estimate probabilities of non-performance with the cumulative distribution functions (CDFs). Therefore, the fragility of a structural system is commonly expressed as a lognormal cumulative distribution function

$$F_R(z) = \Phi\left(\frac{In(z / m_R)}{\xi_R} \right) \qquad (4)$$

where $\Phi(\ )$= standard normal cumulative distribution function; z is the given demand, which is spectral acceleration S_a; m_R is the median capacity; and ξ_R is the logarithmic standard deviation of capacity. Fragility curves can provide information on expected performance at given hazard levels in a concise manner and are easily interpreted by design engineers.

4.1 Peak shear wall displacement

The peak drift responses were obtained from incremental dynamic analyses (IDA). It is noted that under large ground motions, the variability of the peak displacement responses from record to record increased. The reason is that strong ground motions led to high
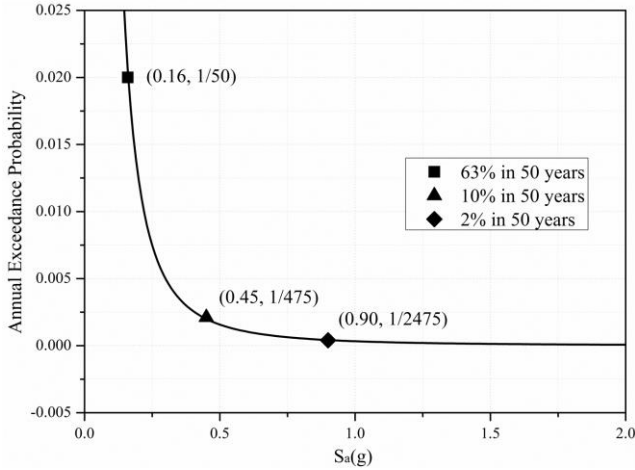
Fig. 7 Seismic hazard curve

Table 3 Failure probabilities and reliability indices obtained from fragility analysis

Hybrid shear wall	Immediate occupancy		Life safety		Collapse Prevention	
	P_f	β	P_f	β	P_f	β
K_r=0.5	3.920×10^{-2}	1.760	4.405×10^{-3}	2.619	9.390×10^{-4}	3.109
K_r=1.0	2.298×10^{-2}	1.996	1.709×10^{-3}	2.927	4.441×10^{-4}	3.324
K_r=2.5	8.307×10^{-3}	2.395	9.174×10^{-4}	3.116	3.243×10^{-4}	3.410
K_r=5.0	6.865×10^{-3}	2.464	5.321×10^{-4}	3.273	2.278×10^{-4}	3.506

nonlinear behavior of the hybrid system which might experience different damage/failure modes. The probability of failure with respect to a specified performance criterion can be determined parametrically by fitting the peak displacement responses to a lognormal distribution. For example, peak shear wall displacements, from the selected group of ground motions scaled to a specific hazard level, were used to form a CDF and to estimate the failure probability. Fig. 5 shows a sample CDF with various lateral infill-to-frame stiffness ratios under the IO limit state. As expected, as the K_r factor increases, the shear wall peak displacement decreases. Using this approach, since the probability of failure is conditioned on a given value of spectral acceleration, and it becomes one point on the fragility curve. Fig. 6 shows the peak displacement fragility curves for the hybrid shear walls with various lateral infill-to-frame stiffness ratios (K_r). The target spectral acceleration values for the three hazard levels (IO, LS, and CP) are also shown in these figures.

When related to different performance objectives, the fragility curves presented here provided a useful tool to evaluate the failure probability of the hybrid shear wall under a specific seismic demand variable (S_a). For instance, with S_a equals to 0.45 g for life safety limit state (LS, 10/50), the failure probabilities for the hybrid shear walls with K_r equal to 0.5, 1.0, 2.5 and 5.0 are 84.3%, 37.2%, 15.3% and 11.2%, respectively. The 10/50 indicates that the seismic hazard corresponding to LS has a 10% probability of exceedance in 50 years. It is found that the failure probability was reduced significantly when stronger infill walls were used. Similar results could be obtained for other hazard levels.

4.2 Seismic hazard and failure probabilities

For a structure or a structural assembly, the general formulation of the failure probability can be described as

$$P_f = \int f_R(z) H_{IM}(z) dz \qquad (5)$$

where $f_R(z)$ is the probability density function of the fragility; $HIM(z)$ is the hazard function of earthquakes with

the intensity measure of S_a. The discrete form of Eq. (5) can be expressed as

$$P_f = \sum \left[F_R(S_{a_i}) - F_R(S_{a_{i-1}}) \right] H_{IM}(S_{a_i}) \qquad (6)$$

where $F_R(S_{a_i})$ is the fragility, and $H_{IM}(S_{a_i})$ is the annual probability of exceeding a given spectral acceleration S_{a_i}, and it can be estimated by a power law relationship as suggested by Cornell *et al.* (2002)

$$H_{IM}(S_a) = k_s S_a^{-k_d} \qquad (7)$$

The IO, LS and CP hazard levels are in correspondence to the earthquake event with a mean return period of 50, 475, and 2,475 years, respectively. The annual spectral acceleration hazard curve $H_{IM}(z)$ was obtained by using Eq. (7) to fit to the S_a values with their corresponding return periods. The regression analysis yielded a value for the decay factor k_d of 2.25273, and a value of 0.00033 for the scale factor k_s. The fitting results are shown in Fig. 7. The failure probabilities for the steel-timber hybrid shear walls were then obtained by Eq. (6). Table 3 summarizes the annual failure probability estimates of exceeding the peak wall displacement limits and the corresponding reliability indices (β). It was also found that under the three performance levels, stronger infill wood shear wall was able to significantly reduce the failure probability of the hybrid shear wall system.

5. Response surface method

Fragility analysis is usually applicable to a given structure under a given seismic hazard level. Response surface methods coupled with common reliability evaluation methods, such as, FORM or importance sampling, are able to consider more random variables. The simulation results obtained from the aforementioned IDA analyses can be fitted by explicit functions that relate the output structural responses of interest to the input intervening random variables. Then, explicit performance functions were established and evaluated by the reliability evaluation methods. The explicit response surface thus provides an effective tool for reliability estimation and optimized design for the steel-timber hybrid structural system.

In this study, the performance function is described as Eq. (8)

$$G = \delta - \Delta(S_a, r, K_r, F_d, \varepsilon) \qquad (8)$$

where δ is the wall drift capacity, calculated as $\delta=H\cdot\theta_{PL}$; H is the wall height and θ_{PL} is the drift ratio limit corresponding to different performance objectives; Δ is the peak drift demand, which is a function of the seismic intensity measure S_a, lateral infill to frame stiffness ratio K_r; design factors of interest F_d (related to shear walls configuration) and the response surface fitting error ε. The intensity measure of ground motions is represented by the spectral accelerations S_a, which was assumed, in accordance with the CCSDB, as a lognormal distribution with mean of 0.115 g and coefficient of variation (COV) of 1.0. The annual Poisson arrival rate of earthquake was assumed as 0.1/year; r represents other characteristics of ground motions and considers the record-to-record variability, and this can be represented by a suite of representative earthquake records. Over the suite of ground motions scaled to one spectral acceleration level and a given K_r, the mean ($\overline{\Delta}_{sm}$) and standard deviation ($\sigma_{\Delta sm}$) of the peak drifts responses were calculated. Therefore, for all the combinations of K_r and Sa, a discrete set of $\overline{\Delta}_{sm}$ and a discrete set of $\sigma_{\Delta sm}$ can be obtained, respectively. Then, polynomial functions, Eq. (9) were used to fit these peak drifts over the domain of random variables, respectively.

$$\overline{\Delta}_{rs} = \sum a_{ijk} S_a^i K_r^j F_d^k \qquad (9a)$$

$$\sigma_{\Delta rs} = \sum b_{ijk} S_a^i K_r^j F_d^k \qquad (9b)$$

where a_{ijk} and b_{ijk} are coefficients evaluated by minimizing the squared error between the polynomial fitting and the model simulation results; and superscripts i, j, and k are the orders of polynomials. Now taking the RS fitting errors into account, the mean $\overline{\Delta}$ and standard deviation σ_{Δ} of the peak responses can be adjusted to

$$\overline{\Delta} = \overline{\Delta}_{rs}(1-\varepsilon_{\overline{\Delta}}) \qquad (11a)$$

$$\varepsilon_{\sigma\Delta}^i = \frac{\sigma_{\Delta rs}^i - \sigma_{\Delta sm}^i}{\sigma_{\Delta rs}^i} \qquad (11b)$$

where $\varepsilon_{\overline{\Delta}}$ and $\varepsilon_{\sigma_{\Delta}}$ are random variables representing RS fitting errors and assumed to follow normal distributions. The errors of the generic ith combination of random variables are calculated by Eq. (11).

The mean and standard deviation of the overall fitting errors can be obtained when all combinations are considered. Using the assumption that peak drift responses follow a lognormal distribution, the performance function Eq. (12) can be rewritten as

$$G = \delta - \frac{\overline{\Delta}}{\sqrt{1+v_{\Delta}^2}} \exp(R_N \sqrt{ln(1+v_{\Delta}^2)}) \qquad (12)$$

where $\overline{\Delta}$ is the mean of peak drift demand; v_{Δ} is the coefficient of variation (COV); and R_N is the standard normal variate R_N (0,1). Once the explicit performance function is obtained, and probability distributions for the random variables are given, the failure probability and

Table 4 Statistical data for peak drifts (mm) from seismic simulation results

$S_a(g)$	Lateral infill to frame stiffness ratio K_r							
	0.5		1.0		2.5		5.0	
	$\overline{\Delta}_{sm}$	$\sigma_{\Delta sm}$	$\overline{\Delta}_{sm}$	$\sigma_{\Delta sm}$	$\overline{\Delta}_{sm}$	$\sigma_{\Delta sm}$	$\overline{\Delta}_{sm}$	$\sigma_{\Delta sm}$
0.10	23.1	10.0	14.6	4.3	9.6	2.3	6.7	3.1
0.16	44.3	23.0	24.2	8.8	15.2	5.8	11.1	4.5
0.30	66.7	27.9	49.3	18.6	34.1	12.9	23.6	8.5
0.45	88.3	34.8	65.0	20.8	47.9	16.9	36.1	13.4
0.60	111.5	39.2	84.8	28.3	65.8	22.4	53.7	18.3
0.75	132.8	46.5	104.9	33.3	86.0	27.3	73.8	20.3
0.90	156.6	54.6	129.9	43.2	110.5	34.5	95.6	23.8
1.05	192.5	65.3	164.3	54.2	137.9	43.5	116.9	27.6
1.20	231.1	78.7	193.8	65.7	162.7	51.7	136.8	35.3
1.35	274.2	93.2	223.5	75.7	186.8	58.2	157.6	42.5
1.50	312.5	104.8	254.5	85.6	211.6	65.3	182.6	48.6
1.65	351.7	118.3	283.2	95.9	234.8	71.4	201.8	53.9
1.80	391.9	131.7	320.7	106.8	261.4	78.7	222.7	60.4
1.95	437.3	144.9	361.4	117.4	292.7	88.3	244.3	67.4
2.10	491.4	162.2	396.4	130.1	324.7	98.4	265.8	72.0

reliability index β can be estimated by first order reliability method FORM.

In this study, for the steel-timber hybrid shear wall system, the performance function considered uncertainties of seismic intensity represented by S_a, lateral infill to frame stiffness ratio K_r and the RS fitting errors, and it can be rewritten as

$$G = \delta - \Delta(S_a, K_r, \varepsilon) \qquad (13)$$

As mentioned before, fifteen spectral acceleration levels and four stiffness ratios (i.e., 0.5, 1.0, 2.5, and 5.0) were used to generate the seismic response database. Table 4 gives the statistics in terms of mean and standard deviations of the peak drifts for all selected combinations of S_a and K_r. Third-order polynomials with nine coefficients were used to fit $\overline{\Delta}_{sm}$ and $\sigma_{\Delta sm}$

$$\overline{\Delta}_{rs} = a_1 S_a K_r + a_2 S_a K_r^2 + a_3 S_a^2 K_r + a_4 S_a^2 K_r^2 + a_5 S_a K_r^3 \\ + a_6 S_a^3 K_r + a_7 S_a^2 K_r^3 + a_8 S_a^3 K_r^2 + a_9 S_a^3 K_r^3 \qquad (14a)$$

$$\sigma_{\Delta rs} = b_1 S_a K_r + b_2 S_a K_r^2 + b_3 S_a^2 K_r + b_4 S_a^2 K_r^2 + b_5 S_a K_r^3 \\ + b_6 S_a^3 K_r + b_7 S_a^2 K_r^3 + b_8 S_a^3 K_r^2 + b_9 S_a^3 K_r^3 \qquad (14b)$$

Fig. 8 shows the polynomial response surfaces with respect to S_a and K_r, as well as the fitted polynomial coefficients. Fig. 9 shows the polynomial fitting errors. Good fitting can be observed, with small fitting errors and most of the data points located near the $45°$ line (the perfect agreement line).

The software RELAN (Foschi *et al.* 2007), was them used to calculate the failure probabilities. Table 5 gives the FORM results of the reliability indices with respect to different K_r values and performance levels. It is noted that
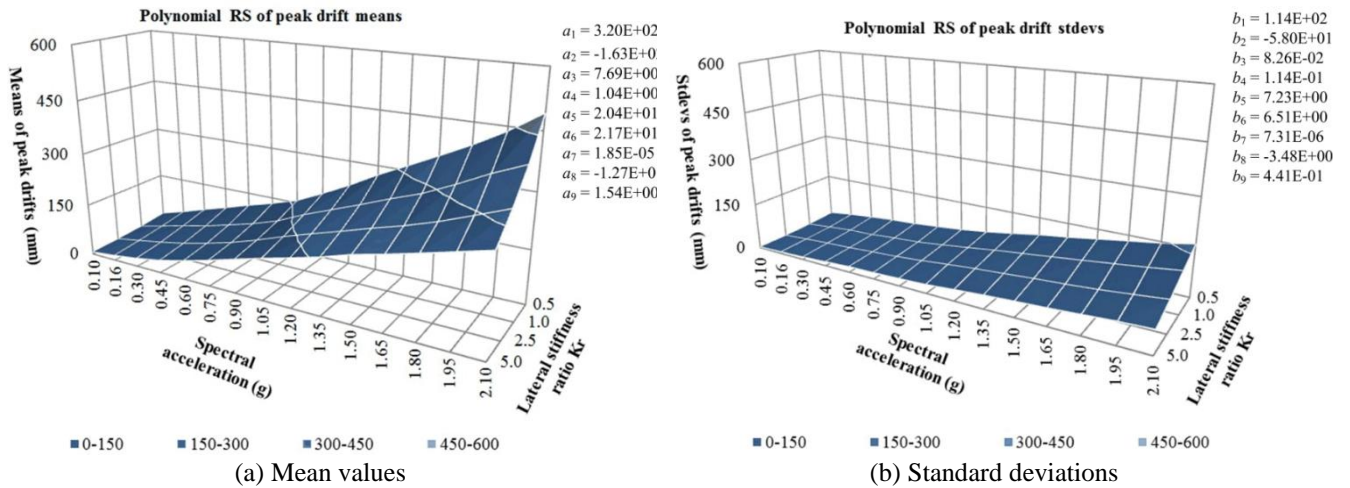
a_1 = 3.20E+02	
a_2 = -1.63E+0	
a_3 = 7.69E+00	
a_4 = 1.04E+00	
a_5 = 2.04E+01	
a_6 = 2.17E+01	
a_7 = 1.85E-05	
a_8 = -1.27E+0	
a_9 = 1.54E+00	

b_1 = 1.14E+02	
b_2 = -5.80E+01	
b_3 = 8.26E-02	
b_4 = 1.14E-01	
b_5 = 7.23E+00	
b_6 = 6.51E+00	
b_7 = 7.31E-06	
b_8 = -3.48E+00	
b_9 = 4.41E-01	

(a) Mean values   (b) Standard deviations

Fig. 8 Simulation data and polynomial RS fitting parameters: (a) Mean values and (b) Standard deviations
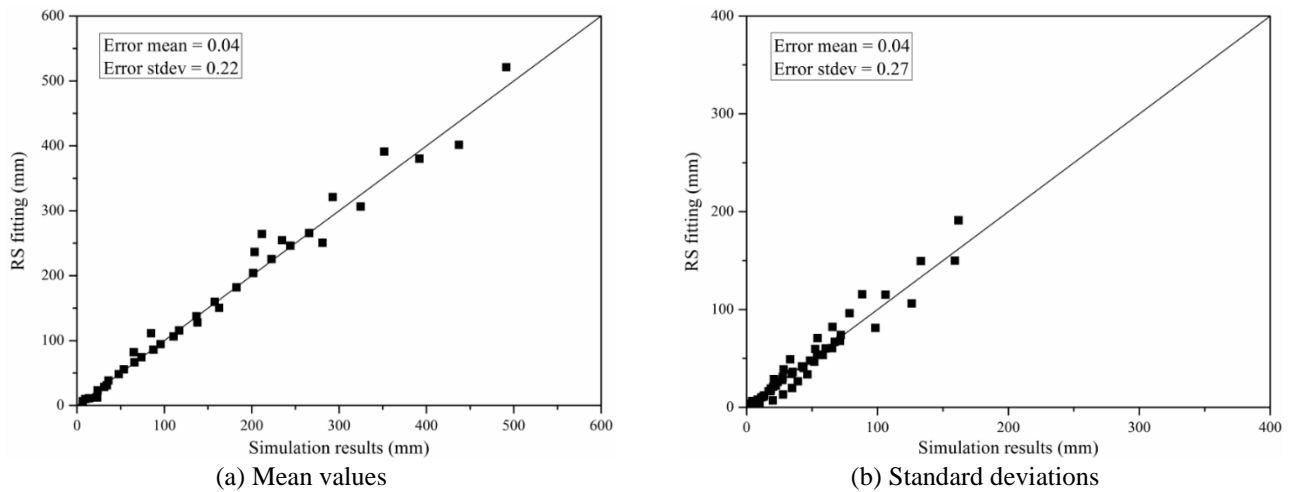

(a) Mean values   (b) Standard deviations

Fig. 9 Polynomial RS fitting results versus simulation results: (a) Mean values and (b) Standard deviations

under a given lateral stiffness ratio K_r, the β value of the IO performance level was between 1.832 and 2.438; for the LS performance level, the β value was between 2.560 and 3.224; and for the CP performance level, the β value was between 3.060 and 3.337. The reliability index increased about 0.73 to 0.82 for the LS limit state comparing with the IO limit state, and it increased by 0.15 to 0.50 for the CP limit state comparing with the LS limit state.

6. Comparision of the results

The seismic reliability of steel-timber hybrid shear wall systems was evaluated using fragility analysis and response surface method with first-order reliability method FORM. A damage assessment process was conducted to determine the performance objectives for steel-timber hybrid shear wall system under different performance levels.

Results showed that although the failure probabilities calculated by the response surface method were slightly higher than those given by the fragility analysis in some cases, the two methods gave very similar results. In the response surface method, a seismic response surface was

Table 5 Failure probabilities and reliability indices obtained from response surface method

Hybrid shear wall	Immediate occupancy		Life safety		Collapse Prevention	
	P_f	β	P_f	β	P_f	β
K_r=0.5	$3.344×10^{-2}$	1.832	$5.237×10^{-3}$	2.560	$1.108×10^{-3}$	3.060
K_r=1.0	$2.071×10^{-2}$	2.039	$2.105×10^{-3}$	2.862	$5.026×10^{-4}$	3.289
K_r=2.5	$9.616×10^{-3}$	2.341	$1.069×10^{-3}$	3.070	$4.433×10^{-4}$	3.324
K_r=5.0	$7.381×10^{-3}$	2.438	$6.331×10^{-4}$	3.224	$3.663×10^{-4}$	3.377

firstly generated by dynamic analyses considering the intervening random variables and design parameters, and the response surface was fitted by polynomial functions. Thus, an explicit performance function was available for failure probability evaluations using FORM. Alternatively, other reliability methods (e.g., importance sampling, Monte Carlo simulation, etc.) can also be used to calculate the failure probabilities. However, when the influence of one source of uncertainties (e.g., ground motions) is much larger than the other sources of uncertainties, fragility analysis appears to be a more straightforward way for the

seismic analysis for a structural system. The fragility method is also very instructive for structural design purposes, and it is less complicated than a fully coupled reliability analysis since it separates the response analysis from the hazard analysis. Both methods can be efficiently used in seismic reliability analysis for the hybrid shear wall systems. The results and reliability methods presented may be used for assessment purposes to evaluate vulnerability or expected damage or, when coupled with loss models, economic losses to steel-timber hybrid structures under seismic hazards in future studies.

7. Conclusions

This paper presents seismic reliability analysis for steel-timber hybrid shear wall systems using two reliability methods. A group of ground motion records was used for nonlinear time-history analyses in order to establish a seismic response database. Performance objectives in terms of peak drift responses were determined according to a damage assessment from reversed cyclic test observations. Fragility curves were constructed in terms of the peak wall drift responses. Given assumptions on seismic hazards, the annual failure probability and reliability indices for the hybrid shear wall systems were obtained. Polynomial fitted peak drift response surfaces were created based on a simulation database from the dynamic analyses, and an explicit performance function was obtained. First-order reliability analysis was then used to calculate the annual failure probabilities for the steel-timber hybrid shear walls with respect to different performance objectives. These two reliability methods gave very similar results and both were believed to be effective in this study.

This study indicated that the relative lateral infill-to-frame stiffness ratio had a strong influence on the seismic performance of the hybrid shear wall system, and the failure probabilities decreased significantly when a stronger infill wood shear wall was used. The reliability-based evaluations and results presented in this paper can provide some insights or suggestions for the performance-based seismic design of such a hybrid shear wall system. The approaches used in this study can also be used as tools to assist the establishment of design specifications for the steel-timber hybrid shear wall systems.

Acknowledgments

References

ASCE/SEI-41. (2013), "Seismic evaluation and retrofit of existing buildings", *American Society of Civil Engineers*, Reston, VA.

Buchanan, A.H., Deam, B., Fragiacomo, M., Pampanin, S. and Palermo, A. (2008), "Multi-storey prestressed timber buildings in New Zealand", *Struct. Eng. Int.*, **18**(2), 166-173.

Chinese Standard GB 50017. (2003), *Code for Design of Steel Structures*, Ministry of Housing and Urban-Rural Development of the People's Republic of China, Beijing, China (in Chinese).

Chinese Standard GB 50011. (2010), C*hinese Code for Seismic Design of Buildings*, National Standard of the People's Republic of China (NSPRC), Beijing, China (in Chinese).

Cornell, C.A., Jalayer, F., Hamburger, R.O. and Foutch, D.A. (2002), "Probabilistic basis for 2000 SAC federal emergency management agency steel moment frame guidelines", *J. Struct. Eng.*, **128**(4), 526-533.

Dickof, C., Stiemer, S.F., Bezabeh, M.A. and Tesfamariam, S. (2014), "CLT-steel hybrid system: ductility and overstrength values based on static pushover analysis", *J. Perform. Constr. Fac.*, **28**(6), A4014012.

Filiatrault, A. and Folz, B. (2002), "Performance-based seismic design of wood framed buildings", *J. Struct. Eng.*, **128**(1), 39-47.

Foliente, G.C. (2000), "Reliability assessment of timber shear walls under earthquake loads", *Proceedings of the 12th World Conference on Earthquake Engineering*, Paper No. 612.

Foschi, R.O., Li, H., Folz, B., Yao, F. and Zhang, J. (2007), "RELAN - Reliability analysis software, V8.0", Univ. of British Columbia, Vancouver, Canada.

Gu, J. and Lam, F. (2004), "Simplified mechanics-based wood frame shear wall model", *Proceedings of the 13th World Conf. on Earthquake Engineering*, Paper No. 3109. Vancouver, Canada.

He, M., Li, Z., Lam, F., Ma, R. and Ma, Z. (2014), "Experimental investigation on lateral performance of steel-timber hybrid shear wall systems", *J. Struct. Eng.*, **140**(4), 04014029.

Kazantzi, A.K., Righiniotis, T.D. and Chryssanthopoulos, M.K. (2008), "Fragility and hazard analysis of a welded steel moment resisting frame", *J. Earthq. Eng.*, **12**(4), 596-615.

Kazantzi, A.K., Righiniotis, T.D. and Chryssanthopoulos, M.K. (2011), "A simplified fragility methodology for regular steel MRFs", *J. Earthq. Eng.*, **15**(3), 390-403.

Li, M. and Lam, F. (2009), "Lateral performance of nonsymmetric diagonal-braced wood shear walls", *J. Struct. Eng.*, **135**(2), 178-186.

Li, M., Lam, F. and Foschi, R.O. (2009), "Seismic reliability analysis of diagonal-braced and structural-panel-sheathed wood shear walls", *J. Struct. Eng.*, **135**(5), 587-596.

Li, Z., He, M., Lam, F., Li, M., Ma, R. and Ma, Z. (2014a), "Finite element modelling and parametric analysis of steel-timber hybrid structures", *Struct. Des. Tall. Spec.*, **23**(14), 1045-1063.

Li, Z., He, M., Li, M. and Lam, F. (2014b), "Damage assessment and performance-based seismic design of steel-timber hybrid shear wall systems", *Earthq. Struct.*, **7**(1), 101-117.

Li, Z., He, M., Ma, Z., Wang, K. and Ma, R. (2016), "In-plane behavior of steel-timber hybrid floor diaphragms: experimental testing and numerical simulation", *J. Struct. Eng.*, **142**(12), 04016119.

Li, Z., Dong, H., Wang, X. and He, M. (2017a), "Experimental and numerical investigations into seismic performance of timber-steel hybrid structure with supplemental dampers", *Eng. Struct.*, **151**, 33-43.

Li, Z., He, M., Wang, X. and Li, M. (2017b), "Seismic performance assessment of steel frame infilled with prefabricated wood shear walls", *J. Constr. Steel. Res.*, DOI: 10.1016/j.jcsr.2017.10.012.

Noh, H.Y., Lignos, D.G., Nair, K.K. and Kiremidjian, A.S. (2012), "Development of fragility functions as a damage classification /prediction method for steel moment-resisting frames using a wavelet-based damage sensitive feature", *Earthq. Eng. Struct. Dyn.*, **41**(4), 681-696.

Pozza, L. and Trutalli, D. (2017), "An analytical formulation of q-factor for mid-rise CLT buildings based on parametric

numerical analyses", *Bull. Earthq. Eng.*, **15**(5), 2015-2033.

Roeder, C., Lumpkin, E., and Lehman, D. (2012), "Seismic Performance Assessment of Concentrically Braced Steel Frames", *Earthq. Spectra*, **28**(2), 709-727.

Sakamoto, I., Kawai, N., Okada, H., Yamaguchi, N., Isoda, H. and Yusa, S. (2004), "Final report of a research and development project on timber based hybrid building structures", *Proceedings of the 8th World Conference on Timber Engineering*, Finnish Association of Civil Engineers, Helsinki, Finland.

Smith, T., Fragiacomo, M., Pampanin, S. and Buchanan, A. (2009), "Construction time and cost estimates for post-tensioned multi-storey timber buildings", *Proc. Inst. Civil Eng. -* Construction Materials, **162**(4), 141-149.

Tesfamariam, S., Stiemer, S.F., Dickof, C. and Bezabeh, M.A. (2014), "Seismic vulnerability assessment of hybrid steel-timber structure steel frame with CLT infill", *J. Earthq. Eng.*, **18**(6): 929-944.

Van de Lindt, J.W., Pryor, S.E. and Pei, S. (2011), "Shake table testing of a full-scale seven-story steel-wood apartment building", *Eng. Struct.*, **33**(3), 757-766.

Wang, C. and Foliente, G.C. (2006), "Seismic reliability of low-rise nonsymmetric woodframe buildings", *J. Struct. Eng.*, **132**(5), 733-744.

Yamaguchi, M., Kawai, N., Murakami, T., Shibata, N. and Namiki, Y. (2004), "Constructions and researches after the project of developing hybrid timber buildings", *Proceedings of the 8th World Conference on Timber Engineering*, Finnish Association of Civil Engineers, Helsinki, Finland.

Zhang, X., Fairhurst, M. and Tannert, T. (2016), "Ductility estimation for a novel timber-steel hybrid system", *J. Struct. Eng.*, **142**(4), E4015001-1-11.

KT